Self-Optimisation of the Final Stage in the Synthesis of EGFR Kinase Inhibitor AZD9291 using an Automated Flow Reactor

Journal:	*Reaction Chemistry & Engineering*
Manuscript ID	RE-ART-03-2016-000059.R1
Article Type:	Paper
Date Submitted by the Author:	04-May-2016
Complete List of Authors:	Holmes, Nicholas; University of Leeds, Chemistry Akien, Geoffrey; Lancaster University Woodward, Robert; AstraZeneca Pharmaceutical Development Meadows, Rebecca; AstraZeneca, Pharmaceutical Development Blacker, John; University of Leeds, Chemistry Bourne, Richard; University of Leeds School of Chemical and Process Engineering

SCHOLARONE™
Manuscripts

ROYAL SOCIETY OF CHEMISTRY

Journal Name

ARTICLE

Self-Optimisation of the Final Stage in the Synthesis of EGFR Kinase Inhibitor AZD9291 using an Automated Flow Reactor

Nicholas Holmes,[a] Geoffrey R. Akien,[ab] A. John Blacker,[ac] Robert L. Woodward,[d] Rebecca E. Meadows[d] and Richard A. Bourne[acd]*

Self-optimising flow reactors combine online analysis with evolutionary feedback algorithms to rapidly achieve optimum conditions. This technique has been applied to the final bond-forming step in the synthesis of AZD9291, an irreversible epidermal growth factor receptor kinase inhibitor developed by AstraZeneca. A four parameter optimisation of a telescoped amide coupling followed by an elimination reaction was achieved using at-line high performance liquid chromatography. Optimisations were initally carried out on a model compound (2,4-dimethoxyaniline) and the data used to track the formation of various impurities and ultimately propose a mechanism for their formation. Our protocol could then be applied to the optimisation of the 2-step telescoped reaction to synthesise AZD9291 in 89% yield.

Introduction

To achieve effective optimisation of a reaction process, careful consideration is needed of the various synergistic interactions that occur between reaction variables such as temperature, reaction time and reagent concentration. It is important to ensure that suitable parameter-defining experiments have been carried out during the course of process development to deliver a robust process that can be easily transferred to a manufacturing facility. Design of experiments (DoE) is a commonly used approach which implements statistical methods to screen and optimise a reaction, particularly for problematic steps. For example, the final step of the synthesis of the Src kinase inhibitor saracatinib, a nucleophilic aromatic substitution between a fluoroaniline and an alcohol, was optimised using a fractional factorial DoE.[1] The optimisation provided enough information about the reaction system to increase the yield by more than 25% on a 300 kg scale. DoE has been used to optimise reaction steps in the synthesis of many pharmaceutical products including vestipitant,[2] raltegravir,[3] otenebant,[4] denagliptin,[5] levovirin,[6] delafloxacin[7] and continuous processes towards doxercalciferol,[8] bendamustime,[9] pyrazinamide[10] and PARP-1 inhibitors.[11]
However, there has been academic development in substituting DoE with evolutionary algorithms in automated

reactors to find optimum conditions. These "self-optimising" reactors incorporate online analysis with a feedback control loop, which uses an optimising algorithm to keep generating new conditions until an optimum is reached. Flow systems are ideally suited for such experimentation, as integration of analytical equipment is facile and measurement and adjustment of operating parameters such as flow rate, temperature and pressure can be accomplished rapidly within a single reactor system.[12] The concept was first introduced by Krishnadasan *et al.*[13] for the synthesis of CdSe quantum dot nanoparticles in microreactors with online UV and SNOBFIT (Stable Noisy Optimisation by Branch and Fit) algorithm.[14] Latterly the Jensen,[15, 16] Poliakoff,[17, 18] and Cronin[19] groups have combined online chromatography and spectroscopy, with simplex algorithms[20] for the optimisation of small organic molecules. This article demonstrates the applicability of using this approach for complex systems including telescoped reactions for the synthesis of pharmaceuticals.

Herein is described the optimisation, using an automated reactor and adaptive feedback control, of the final bond-forming step in the synthesis of **3** (AZD9291 acrylamide, generic name osimertinib), an irreversible epidermal growth factor receptor (EGFR) kinase inhibitor (**Error! Reference source not found.**).[21] The reactor set-up includes 3 separate reagent pumps, which meet in two mixing tees before entering the tubular reactor. The reaction mixture leaves the reactor through a filter then enters a sample loop, which delivers an aliquot of reaction mixture to the mobile phase of the HPLC, without prior quench or dilution. The whole reactor is maintained under fixed back-pressure. The reactor has active heating and cooling, significantly reducing the time taken to reach the set conditions and is controlled by a custom written MatLab program and optimised using the SNOBFIT algorithm.[14]

Comment [NH1]: Rev 1, comment D

[a.] *Institute of Process Research and Development, School of Chemistry, University of Leeds, Leeds, LS2 9JT, UK. E-mail: r.a.bourne@leeds.ac.uk*
[b.] *Department of Chemistry, Faraday Building, Lancaster University, Lancaster,LA1 4YB, UK*
[c.] *c School of Chemical and Process Engineering, University of Leeds, Leeds,LS2 9JT, UK.*
[d.] *AstraZeneca Pharmaceutical Development, Silk Road Business Park, Macclesfield, SK10 2NA, UK.*
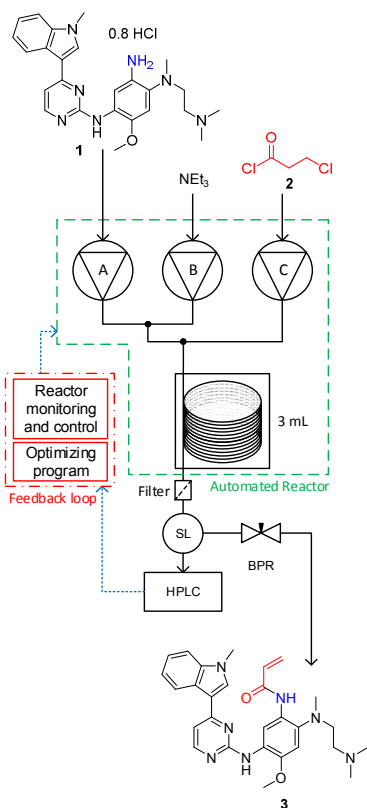
Figure 1. An automated flow reactor with adaptive feedback control and optimisation algorithm (see ESI for full experimental details). The reagents are fed into the reactor using piston pumps and meet in two separate tee-pieces. The reaction stream leaves the reactor through a filter and is sampled by a sample loop (SL) with online HPLC before the product is collected. The reactor is maintained under fixed 250 psi back pressure. Reaction monitoring and feedback control is carried out using a MatLab interface. The SNOBFIT algorithm calculates conditions based on the calculated HPLC yield.

SNOBFIT is a branch and fit algorithm that plots random points until there is enough data to fit a polynomial to improve on the existing optimum. It is then able to generate new sets of conditions to concurrently improve on the optimum or polynomial fit; or explore empty space. The algorithm was chosen as it generates a scatter of data across the experimental area so a response surface can also be fitted in addition to the optimisation.
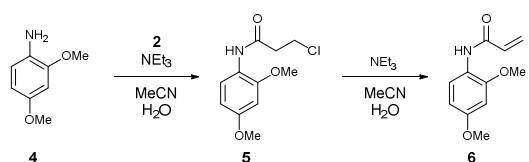
Scheme 1. Synthesis of the model acrylamide **6** *via* the β-chloroamide **5** intermediate.

Results and Discussion

Model Optimisation

Initial optimisations were carried out on a model compound, 2,4-dimethoxyaniline **4**, to gain understanding of the reaction without consuming high value material and provide initial boundary conditions for the AZD9291 optimisation. The reaction proceeds *via* formation of the β-chloroamide **5** by a base mediated reaction of the aniline **4** with acid chloride **2**, followed by elimination to yield the acrylamide **6** (**Error! Reference source not found.**). Aniline **1** is highly nucleophilic due to the high electron density on the aromatic ring and so it was important to choose a model aniline with electron donating groups. A solvent composition of acetonitrile and water (7:2, v:v) was used for the pump reservoir solutions, with the exception of the acid chloride, which was prepared in anhydrous acetonitrile. This was selected according to the current batch procedure for synthesising **3**. Although competing hydrolysis of the acid chloride occurred in the reaction mixture, an aqueous solution was required to dissolve the resultant triethylammonium chloride.

The reaction yield, measured using at-line HPLC, was optimised using the SNOBFIT algorithm, with the flow rate of the aniline **4** (pump A), molar equivalents of acid chloride **2** (pump C - wrt aniline), triethylamine (pump B – eq, wrt acid chloride) and the reactor temperature as variables. An excess of triethylamine was used to ensure there was sufficient to quench the HCl. Other reaction variables such as substrate concentration and residence time are confounded within the flow rates and equivalents, therefore contributing to the algorithms choice of optimum conditions without increasing the computational expense of added variables. An internal standard of biphenyl was added to the aniline solution for the algorithm to calculate a real-time yield by maximising the ratio between the acrylamide **6** and biphenyl peaks. Percentage yields are quoted as HPLC area % of aniline derived material. The optimisation variable limits are displayed in **Error! Reference source not found.**.

Table 1. Optimisation condition limits for the model aniline reaction.

Limit	Pump A /mL min^{-1}	Pump B /eq	Pump C /eq	Temperature /°C
Min	0.100	4.5	0.9	0
Max	0.500	20	2.1	130

Pump A reservoir 0.241 mol L^{-1} aniline **4**, 0.0156 mol L^{-1} biphenyl, pump B reservoir 3.73 mol L-1 triethylamine, pump C reservoir 1.00 mol L-1 acid chloride **2**.

It was important to include material minimisation steps to reduce flows whilst waiting for the reactor temperature to be reached and equilibrate (**Error! Reference source not found.**). This ensured that minimal costly material was not wasted whilst the reactor was reaching temperature. The Polar Bear Plus reactor used has active cooling which significantly decreased the time required to reduce the temperature. Waiting for the reactor to reach temperature was the biggest contribution to the overall optimisation duration and

Comment [NH3]: Rev 1, comment A

Comment [NH4]: Rev 1, comment A

Comment [NH5]: Rev 1, comment B

Comment [NH6]: Rev 1, comment C

Comment [NH2]: Rev 2, comment 2

ultimately influenced the decision to use the SNOBFIT algorithm. The algorithm generates sets of experiments, configured to be of 4/5, and these were performed in order of ascending temperature. HPLC was used for analysis as it is ideally suited for quantification of the complex range of species generated. Other work has used analyses with much shorter acquisition times,[16, 18, 19, 22] but due to the complex mixture would require detailed chemometric modelling to enable quantification. Due to the sets of experiments delivered by the SNOBFIT algorithm, conditions could be set and next reaction started as soon as the HPLC sample was introduced, and therefore before analysis was completed, and so the HPLC analysis had a very minor effect on the overall optimisation duration.

Figure 3. Multi-dimensional plot of the optimisation of acrylamide 6. The 3-axis plot show the aniline 4 flow rate (x-axis), acid chloride 2 eq (y-axis) and temperature (z-axis). The size of the point represents the molar eq of NEt₃, and the colour represents the product yield. The optimum conditions: 12.2 min, 117.8 °C, 16 eq NEt₃, 1.7 eq 2 are highlighted by the star.
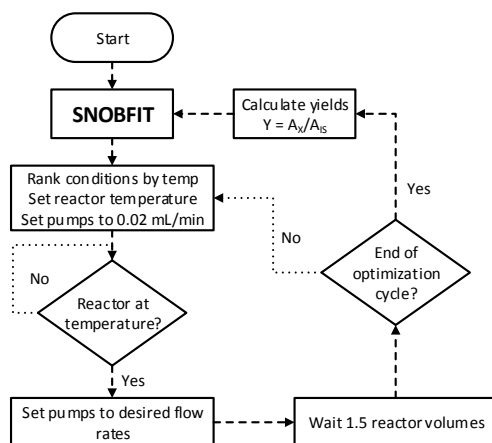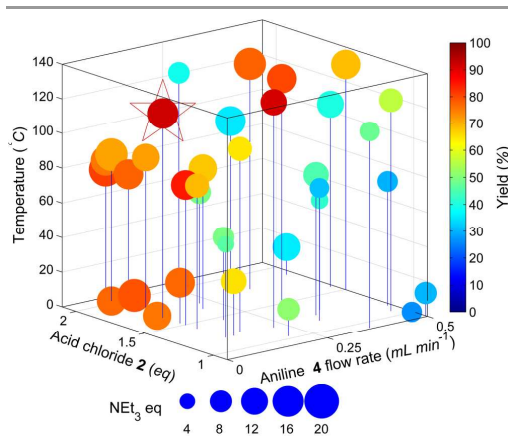

Figure 2. Conditions generated by SNOBFIT in each algorithm cycle were ranked in ascending temperature to minimise the time taken for heating and cooling. Whilst the reactor was reaching temperature, all the pumps were set to 0.02 mL/min. When the reactor was at the desired temperature, the correct flow rates were set. A real-time yield was calculated using the ratio between the product and biphenyl HPLC peaks (Y=yield, A_x = area of 6 or 3, A_{IS} = area of biphenyl).

The results of the yield optimisation are displayed in **Error! Reference source not found.**. The optimum conditions are 0.1 mL/min 4, 117.8 °C, 1.7 equivalents of 2, 16 equivalents of triethylamine and a residence time of 12.2 min, generating 6 in a 92% yield. A low aniline flow rate correlates to an increase in the residence time and higher yields are achieved at higher temperatures. The excess of 2 is likely to compensate for the competing hydrolysis reaction and high equivalents of triethylamine are possibly required to accelerate the slower elimination step. Further scrutiny of the HPLC chromatograms show >99% conversion of 4 in each reaction with the other main component being the intermediate 5, highlighting that the elimination step is probably rate limiting. In the optimum chromatogram, complete conversion of 4 is achieved with the resulting impurities totalling 8% (2.7% 5). Prior to the optimisation, a batch synthesis of 6 generated the desired product in 76 % isolated yield with 1.5 eq 2, 2.5 eq NEt₃ and stirring at 0 °C for 3 hours.
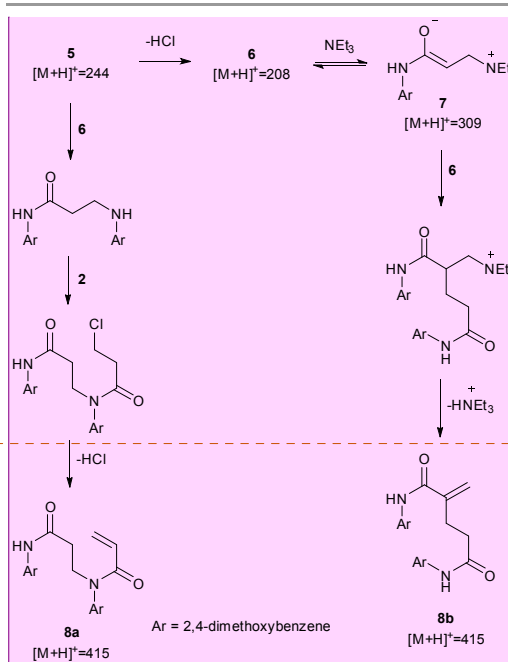
Scheme 2. Proposed mechanisms to dimers 8a and 8b. The observation of a peak corresponding to 7 suggested a Rahut-Currier mechanism to 8b but subsequent LC-MS-MS analysis showed the major dimer to most likely be 8a. All observed peaks from offline LC-MS are displayed.

Impurity identification and optimisation

Using the optimisation data, it was possible to create multi-dimensional plots for all the significant impurities observed by HPLC, and find the experimental space where impurity yield is

Comment [NH9]: Rev 2, Comment 3

Comment [RB7]: Rev 1, comment 3

Comment [NH8]: Rev 2, comment 1

high. These were identified using offline LC-MS and by comparing the relative retention times with known impurity standards in the AZD9291 HPLC method. An impurity of particular concern in the AZD9291 route was known to be a dimer. In our model system, a dimeric impurity with a molecular weight equivalent to two monomers of **6** was also detected. Two potential mechanisms were proposed leading to dimeric species: nucleophilic substitution between **5** and **4** followed by amidation with **2** and subsequent elimination to give dimer **8a**; and a Rahut-Currier mechanism[23] (a variation on the Baylis-Hillman reaction)[24] *via* the enolate **7** to give dimer **8b** (**Error! Reference source not found.**). One of the impurities in the LC-MS analysis had a mass of m/z 309 and further LC-MS-MS analysis showed a fragment of m/z 208 in the second MS spectrum. These data suggest that this impurity is the enolate **7**. LC-MS-MS analysis of the dimer showed a peak at m/z 437 corresponding to the Na adduct of **8** and a fragment at m/z 230 suggesting loss of the acrylamide fragment only found in dimer **8a** indicating that nucleophilic substitution is the route to the undesired dimer.
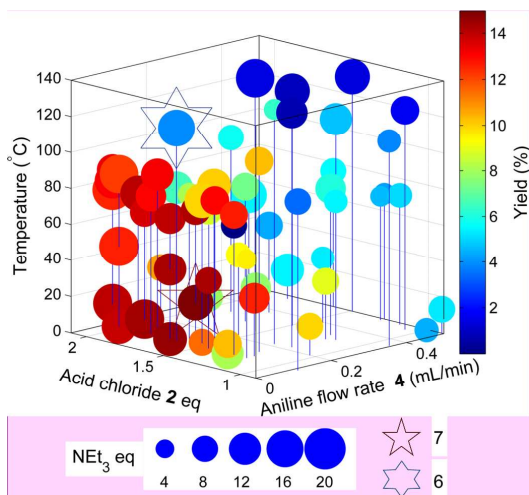

Figure 4. Multi-dimensional plot, showing the results of the optimization of enolate **7**. The 3-axis plot show the aniline **4** flow rate (x-axis), acid chloride **2** eq (y-axis) and temperature (z-axis). The size of the point represents NEt$_3$ eq, and the colour represents the product yield. The optimum conditions: 0.1 mL min^{-1} **4**, 117.8 °C, 1.5 eq **2**, 15.2 eq NEt$_3$ and 12.7 min are highlighted by the 5-pointed star. The optimum conditions of **6** are highlighted by the 6-pointed star.

Another optimization was run, to maximize the amount of **7**, and find experimental regions where the impurity formation is high. The yields of the impurity from the original optimization were inputted to SNOBFIT as preliminary data and the algorithm continued from the last data set shown in **Error! Reference source not found.**.
Unsurprisingly, the optimum region of **7** (Figure 4) is similar to that of the acrylamide **6**, as the acrylamide is a precursor for the formation of the enolate. However, **7** is formed in higher yields at much lower temperatures, most likely due to

increased temperatures favouring the acrylamide **6** in this equilibrium.
Despite the increased yields obtained through the optimisation, it was not possible to isolate enolate **7** for full characterisation.

Table 2. Optimisation condition limits for the AZD9291 acrylamide reaction.

Limit	Pump A /mL min^{-1}	Pump B /eq	Pump C /eq	Temperature /°C
Min	0.080	2.2	0.75	80
Max	0.150	15	3.0	150

Pump A reservoir 0.136 mol L^{-1} aniline **1**, 0.0255 mol L^{-1} biphenyl, pump B reservoir 1.20 mol L^{-1} triethylamine, pump C reservoir 0.500 mol L^{-1} acid chloride **2**.

AZD9291 acrylamide optimisation

The data obtained from the model compound was used for designing the optimisation of AZD9291 acrylamide **3**. The same reactor set-up and reaction route was used as the above transformations, with the exception of the aniline substrate used. A solution of the hydrochloride salt of **1** (0.8 HCl) was used as the free aniline had very low solubility in the solvent mixture. The optimisation limits are displayed in **Error! Reference source not found.**, the flow rates of which correspond to a calculated residence time between 4 and 22 minutes. The temperature range has increased from the model compound as poor conversion of **1** was achieved during initial experiments at lower temperatures.
The results of the yield optimisation are displayed in Figure 5. The optimum conditions (0.11 mL/min **1**, 2.65 eq **2**, 10.5 eq NEt$_3$, 123.9 °C, 9.36 min in 89%) are slightly different to that of the model compound. The optimum point for our model system was at the lowest flow rate of the aniline, thereby maximising the residence time, however, the flow rate of **1** is towards the middle of the limits. Figure 4 shows a clear interrelationship between the flow rate of **1** and the temperature required for high yield. The productivity of the reactor system can be significantly increased, if the flow rate of **1** is increased a corresponding increase in reaction temperature can be used to maintain a high yield with only marginal decreases from the maximum observed yield.
The optimum region requires high equivalents of **2** unlike the model compound and exhibits a higher temperature dependence. This is possibly due to the lower reactivity of **1** compared to the less substituted model compound resulting in greater competition from the hydrolysis of **2**. In addition the pre-equilibrium (to deprotonate the HCl salt of **1**) and amide coupling steps may be mixing sensitive and may consequently require high flow rates through the mixing tees as mixing increases with flow rate through a tee-piece.[25] The material minimisation functions improved the efficiency of material use, calculations showed a reduction in material use of 22%.
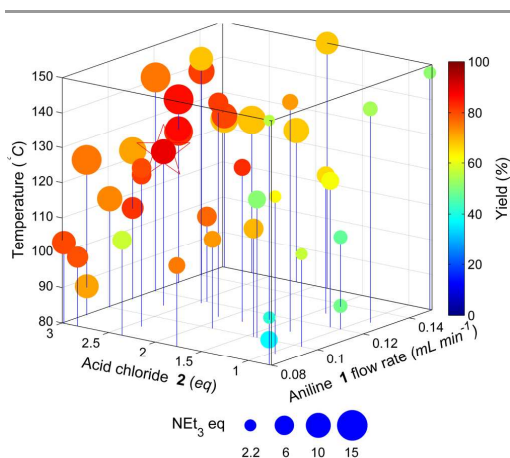
Figure 5. Multidimensional plot of the optimisation of acrylamide 3. The 3 axis flow rate shows the aniline 1 flow rate (x-axis), acid chloride 2 eq (y-axis) and temperature (z-axis). The size of the point corresponds to the molar eq of NEt3, the color is the yield. Optimum conditions: 9.36 min, 123.9 °C, 10.5 eq NEt3, 2.7 eq 1 are highlighted by the star.

Conclusions

Presented is the novel application of implementing a self-optimising automated flow reactor for a 2-step telescope in the synthesis of an active pharmaceutical ingredient. The concept was tested on a model substrate, which aided experimental set-up and data analysis for the optimisation of **3**. The model optimisations also provided enough information to be able to predict impurity formation mechanisms and optimised the synthesis of the model compound **6** to a yield of 92%. The second optimisation provided conditions to generate **3** in 89% yield. Overall, the rapid automated optimisation of **3** required 42 separate experiments, which used 10 g of material and overall run time of 26 hours (average of ~240 mg per experiment). The use of self-optimising systems allows swift exploration and process optimisation even of multistage reaction systems without human intervention. Crucially, this enables researchers to focus their effort on the scientifically challenging aspects whilst the automation system performs the routine experimentation.

Acknowledgements

References

1. S. A. Raw, B. A. Taylor and S. Tomasi, *Org. Process Res. Dev.*, 2011, **15**, 688-692.
2. G. Guercio, S. Bacchi, M. Goodyear, A. Carangio, F. Tinazzi and S. Curti, *Org. Process Res. Dev.*, 2008, **12**, 1188-1194.
3. G. R. Humphrey, P. J. Pye, Y.-L. Zhong, R. Angelaud, D. Askin, K. M. Belyk, P. E. Maligres, D. E. Mancheno, R. A. Miller, R. A. Reamer and S. A. Weissman, *Org. Process Res. Dev.*, 2010, **15**, 73-83.
4. J. A. Ragan, D. E. Bourassa, J. Blunt, D. Breen, F. R. Busch, E. M. Cordi, D. B. Damon, N. Do, A. Engtrakul, D. Lynch, R. E. McDermott, J. A. Mongillo, M. M. O'Sullivan, P. R. Rose and B. C. Vanderplas, *Org. Process Res. Dev.*, 2009, **13**, 186-197.
5. R. B. Appell, L. T. Boulton, E. D. Daugs, M. Hansen, C. H. Hanson, J. Heinrich, C. Kronig, R. C. Lloyd, D. Louks, M. Nitz, C. Praquin, J. A. Ramsden, H. Samuel, M. Smit and M. Willets, *Org. Process Res. Dev.*, 2012, **17**, 69-76.
6. P. Zhang, Z. E. Dong and T. P. Cleary, *Org. Process Res. Dev.*, 2005, **9**, 583-592.
7. R. Hanselmann, G. Johnson, M. M. Reeve and S.-T. Huang, *Org. Process Res. Dev.*, 2008, **13**, 54-59.
8. B. G. Anderson, W. E. Bauta and W. R. Cantrell, *Org. Process Res. Dev.*, 2012, **16**, 967-975.
9. J. Chen, K. Przyuski, R. Roemmele and R. P. Bakale, *Org. Process Res. Dev.*, 2014, **18**, 1427-1433.
10. R. J. Ingham, C. Battilocchio, J. M. Hawkins and S. V. Ley, *Beilstein J. Org. Chem.*, 2014, **10**, 641-652.
11. P. Filipponi, C. Ostacolo, E. Novellino, R. Pellicciari and A. Gioiello, *Org. Process Res. Dev.*, 2014, **18**, 1345-1353.
12. N. Holmes and R. A. Bourne, in *Chemical Process Technology for a Sustainable Future*, eds. T. M. Letcher, J. L. Scott and D. A. Paterson, RSC Publishing, 1st edn., 2014, ch. 3, pp. 28-45; M. Rasheed and T. Wirth, *Angew. Chem., Int. Ed.*, 2011, **50**, 357-358; S. V. Ley, D. E. Fitzpatrick, R. J. Ingham and R. M. Myers, *Angew. Chem. Int. Ed.*, 2015, **54**, 3449-3464; S. V. Ley, D. E. Fitzpatrick, R. M. Myers, C. Battilocchio and R. J. Ingham, *Angew. Chem., Int. Ed.*, 2015, **54**, 10122-10136; D. C. Fabry, E. Sugiono and M. Rueping, *React. Chem. Eng.*, 2016, doi: 10.1039/C5RE00038F.
13. S. Krishnadasan, R. J. C. Brown, A. J. de Mello and J. C. de Mello, *Lab Chip*, 2007, **7**, 1434-1441.
14. W. Huyer and A. Neumaier, *ACM Trans. Math. Softw.*, 2008, **35**, 1-25.
15. J. P. McMullen and K. F. Jensen, *Org. Process Res. Dev.*, 2010, **14**, 1169-1176; J. P. McMullen, M. T. Stone, S. L. Buchwald and K. F. Jensen, *Angew. Chem., Int. Ed.*, 2010, **49**, 7076-7080; B. J. Reizman and K. F. Jensen, *Chem. Commun.*, 2015, **51**, 13290-13293.
16. J. S. Moore and K. F. Jensen, *Org. Process Res. Dev.*, 2012, **16**, 1409-1415.
17. A. J. Parrott, R. A. Bourne, G. R. Akien, D. J. Irvine and M. Poliakoff, *Angew. Chem., Int. Ed.*, 2011, **50**, 3788-

3792; R. A. Bourne, R. A. Skilton, A. J. Parrott, D. J. Irvine and M. Poliakoff, *Org. Process Res. Dev.*, 2011, **15**, 932-938; D. N. Jumbam, R. A. Skilton, A. J. Parrott, R. A. Bourne and M. Poliakoff, *J. Flow Chem.*, 2012, **2**, 24-27; Z. Amara, E. S. Streng, R. A. Skilton, J. Jin, M. W. George and M. Poliakoff, *Eur. J. Org. Chem.*, 2015, **2015**, 6141-6145.

18. R. A. Skilton, A. J. Parrott, M. W. George, M. Poliakoff and R. A. Bourne, *Appl. Spectrosc.*, 2013, **67**, 1127-1131.

19. V. Sans, L. Porwol, V. Dragone and L. Cronin, *Chem. Sci.*, 2015, **6**, 1258-1264.

20. W. Spendley, G. R. Hext and F. R. Himsworth, *Technometrics*, 1962, **4**, 441-461; J. A. Nelder and R. Mead, *Comput. J.*, 1965, **7**, 308-313; M. W. Routh, P. A. Swartz and M. B. Denton, *Anal. Chem.*, 1977, **49**, 1422-1428.

21. M. R. V. Finlay, M. Anderton, S. Ashton, P. Ballard, P. A. Bethel, M. R. Box, R. H. Bradbury, S. J. Brown, S. Butterworth, A. Campbell, C. Chorley, N. Colclough, D. A. E. Cross, G. S. Currie, M. Grist, L. Hassall, G. B. Hill, D. James, M. James, P. Kemmitt, T. Klinowska, G. Lamont, S. G. Lamont, N. Martin, H. L. McFarland, M. J. Mellor, J. P. Orme, D. Perkins, P. Perkins, G. Richmond, P. Smith, R. A. Ward, M. J. Waring, D. Whittaker, S. Wells and G. L. Wrigley, *J. Med. Chem.*, 2014, **57**, 8249-8267; D. Cross, S. Ashton, C. Nebhan, C. Eberlein, M. R. V. Finlay, G. Hughes, V. Jacobs, M. Mellor, M. Red Brewer, C. Meador, J. Orme, P. Spitzler, S. Powell, A. Rahi, P. Taylor, R. A. Ward, P. Daunt, A. Galer, T. Klinowska, G. Richmond and W. Pao, *Mol. Cancer Ther.*, 2013, **12**, A109; D. Wilson, C. Finnie and S. A. Raw, WO2015101791A1, 2015.

22. D. E. Fitzpatrick, C. Battilocchio and S. V. Ley, *Org. Process Res. Dev.*, 2015, doi: 10.1021/acs.oprd.5b00313; N. Holmes, G. R. Akien, R. J. D. Savage, C. Stanetty, I. R. Baxendale, A. J. Blacker, B. A. Taylor, R. L. Woodward, R. E. Meadows and R. A. Bourne, *React. Chem. Eng.*, 2016, **1**, 96-100.

23. M. M. Rauhut and H. Currier, *US. Pat.*, US3074999, 1963.

24. D. Basavaiah, A. J. Rao and T. Satyanarayana, *Chem. Rev.*, 2003, **103**, 811-892; A. B. Baylis and M. E. D. Hillman, *Ger. Pat.*, DE2155113 (A1), 1972; A. B. Baylis and M. E. D. Hillman, *US. Pat.*, US3743669 (A), 1973.

25. K. D. Nagy, B. Shen, T. F. Jamison and K. F. Jensen, *Org. Process Res. Dev.*, 2012, **16**, 976-981; S. Schwolow, J. Hollmann, B. Schenkel and T. Röder, *Org. Process Res. Dev.*, 2012, **16**, 1513-1522.

Supporting Information

Self-Optimization of the Final Stage in the Synthesis of EGFR kinase inhibitor AZD9291 using an Automated Flow Reactor

Nicholas Holmes, Geoffrey Akien, A. John Blacker, Robert L. Woodward, Rebecca E. Meadows and Richard A. Bourne*

Contents

1 Chemicals

All chemicals were commercially available and used without further purification, unless otherwise stated: 2,4-dimethoxyaniline (Maybridge, 97%), triethylamine (Acros 99%), 3-chloropropionyl chloride (Acros 98%), hydrochloric acid (Fisher, 37%) biphenyl (Aldrich, 99.5% GC), acetonitrile (VWR, 99.9%). Anhydrous acetonitrile was obtained from departmental solvent purification system with a water content of 2.6 ppm. AZD9291 aniline **1** was supplied by AstraZeneca PLC.

2 Equipment

2.1 Automated Reactor

Reagents were pumped using Jasco PU980 dual piston HPLC pumps and streams were mixed using Swagelok SS-100-3 tee-pieces. A 3 mL reactor was fitted to a Cambridge Reactor Design Polar Bear Flow Synthesizer and the outlet was filtered with a Swagelok SS-2F-2 inline filter. Sampling was achieved using a VICI Valco EUDA-CI4W.06 sample loop with 0.06 µL injection volume. The reactor was maintained under fixed back pressure using an Upchurch Scientific 250 psi back pressure regulator. Polyflon PTFE tubing (1/16" OD, 1/32" ID) was used throughout the reactor. Glassware for anhydrous solutions was dried in an oven at 120 °C.
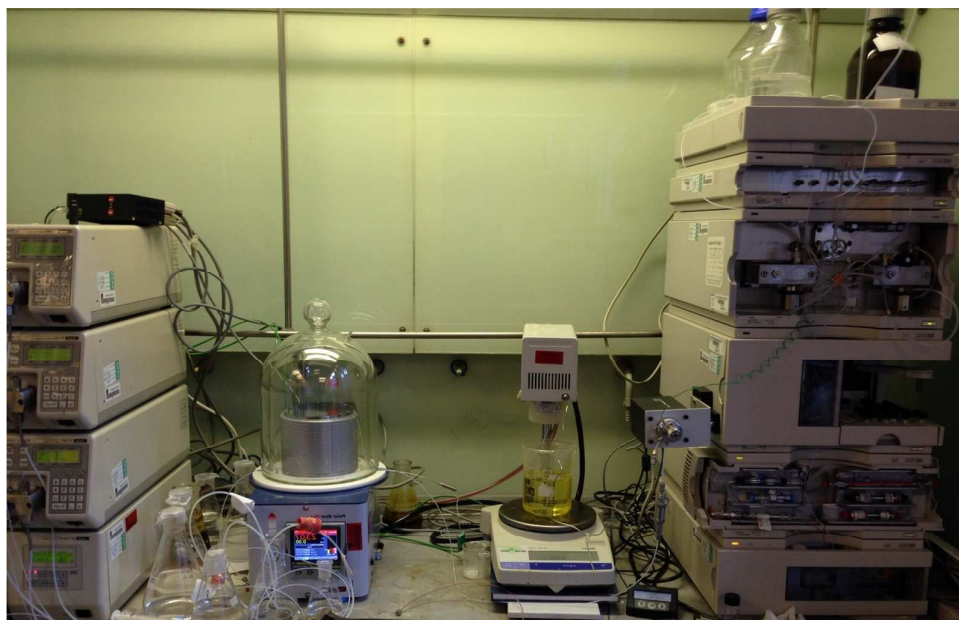
Figure S1 - Photo of automated flow reactor
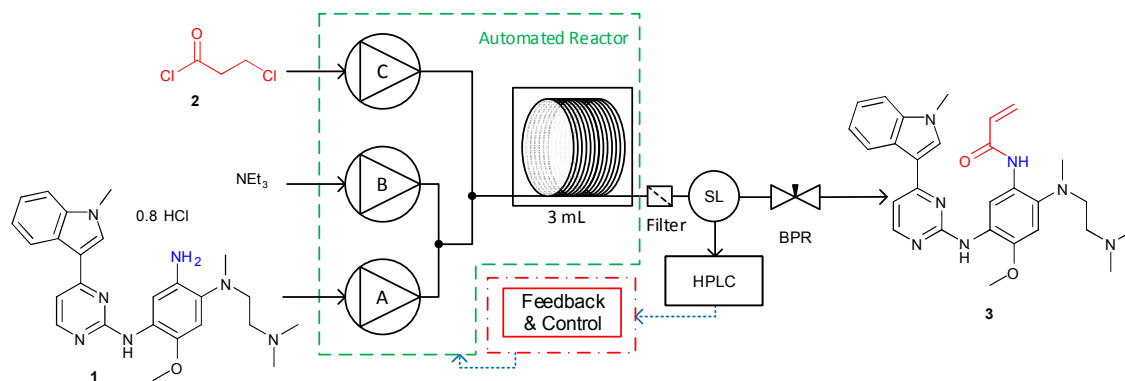
Figure S2 - Schematic for the automated reactor. The reagents are introduced to the reactor using dual piston pumps (A,B and C) with the pump streams mixing in consecutive mixing tees. The reactor outlet passes through an inline filter before being sampled for HPLC analysis. The whole reactor is maintained under a fixed back-pressure to prevent boiling at temperatures above the solvent boiling point

2.2 Optimization Procedure

An optimization program was written in MatLab that controlled the pump flow rates and reactor temperature; determined steady state; calculated a product yield; and controlled the inputs and outputs to and from the SNOBFIT algorithm. Whilst the reactor was reaching temperature, the pumps were set to 0.020 mL min^{-1}. When the reactor was at temperature, the pumps were set to the flow rates calculated by the algorithm and pumped for 1.5

residence times. When the reactor was at steady state, a HPLC sample was taken and the optimization moved on to the next experiment (Figure S3).
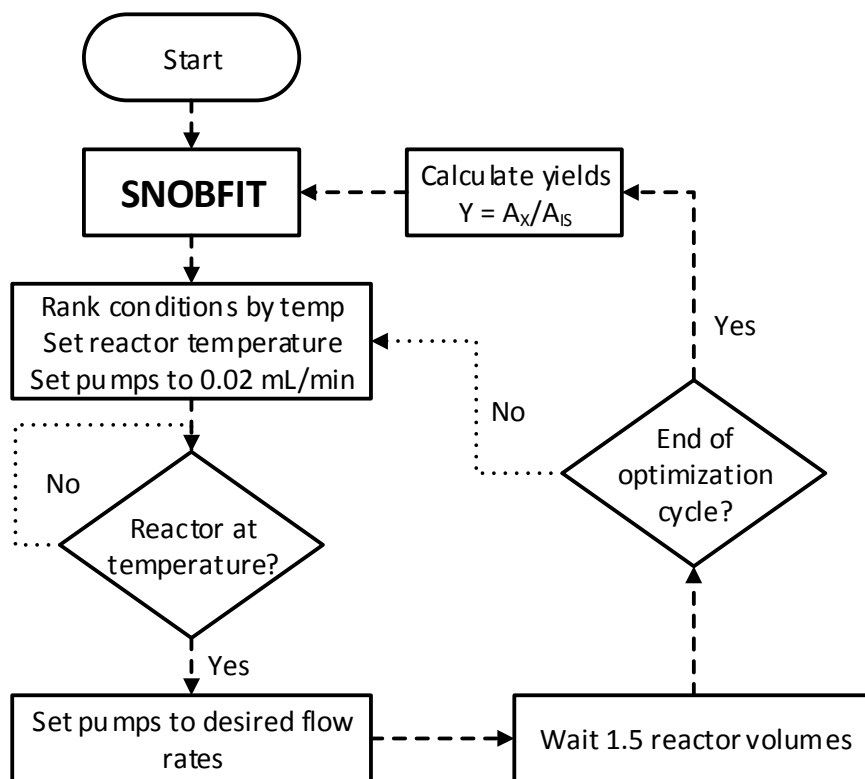
Figure S3 – Flow chart showing the important steps during the optimization program.

Automated yield analysis was calculated during optimizations by calculating the ratio between the desired product and internal standard peak, from HPLC. The SNOBFIT algorithm is a minimizing algorithm and was thus set to maximize the negative of this ratio. This number was translated to a product yield (after completion of the full optimization) by internally normalizing it against the ratio of all other aniline species peak areas and assuming that all aniline species had the same response factor. This was necessary as the small amounts of impurities would be impossible to isolate in quantities suitable for separate calibration runs. Summation of the normalized peak areas for all aniline compounds showed consistent mass balance (100 +/- 6% in both the AZD9291 studies and 100 +/- 7% with the model aniline **4**).

2.3 Analytical

NMR analysis was carried out using a Bruker 500 MHz fourier transform machine. Chemical shifts are quoted as parts per million (ppm) with reference to an internal solvent peak of $SiMe_4$ (TMS). Peaks are quoted as s (singlet), br s (broad singlet) d (doublet), t (triplet), variations thereof (e.g. dd doublet of doublets, dt doublet of triplets etc.) or multiplet (m).

Accurate mass MS was carried out using a Bruker MaXis Impact. IR was collected using a Bruker Alpha FT-IR. Copies of the NMR analysis is available at the end of the document.

At-line HPLC analysis was carried out using an Agilent 1100 HPLC. Method 1: Sigma Ascentis Express C18 (50 x 6.6 mm, 2.7 µm) column; A 0.1 % (v:v) aqueous trifluoroacetic acid, B 0.1 % (v:v) trifluoroacetic acid in acetonitrile; 5% to 95% B over 8.5 mins, to 5% B after 9.5 mins, post time 30 s; 1.2 mL min^{-1}, 254 nm, 20 °C. Method 2: Waters X-Bridge C18 (150 x 30 mm, 3.5 µm) column; A water, B acetonitrile, C 10% (v:v) aqueous trifluoroacetic acid; 5% to 38% B over 10 mins, to 95% B after 15 mins to 5% B after 15.1 mins, 3% C hold over 15.1 mins, post time 3 mins (5% B, 3% C); 1.0 mL min^{-1}, 210 nm, 40 °C. Offline LC-MS was obtained using an Agilent 1200 UHPLC and Bruker HCTultra Ion Trap Spectrometer.
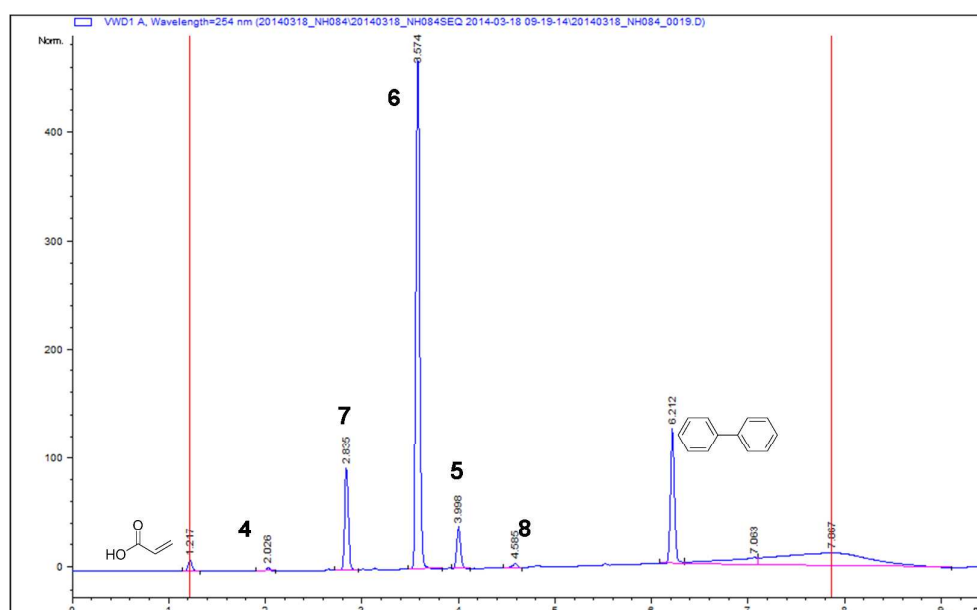
Figure S4 – Example HPLC for the model reaction (Method 1)
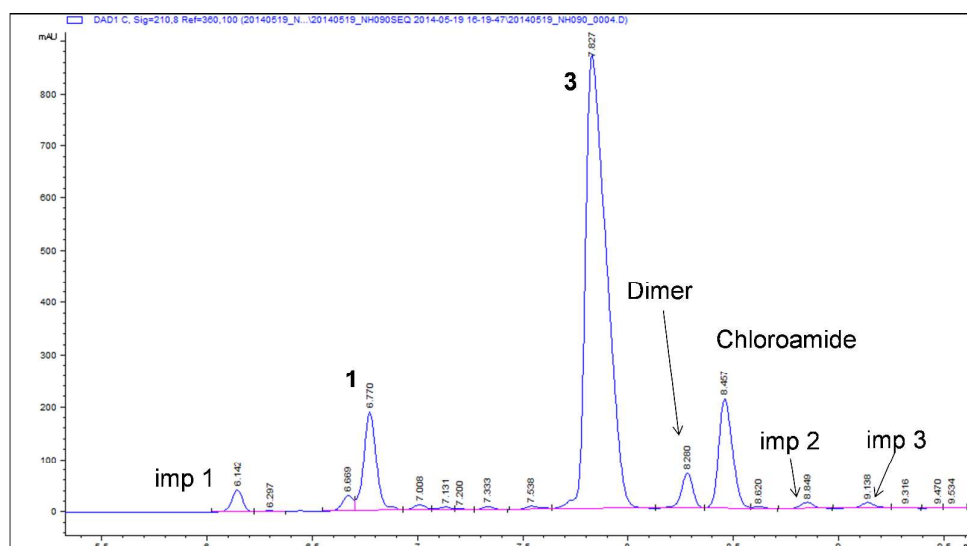
Figure S5 – Example HPLC for the AZD9291 reaction (Method 2) from 5.5 to 9.5 mins. The major impurities are labelled as imp 1-3.

3   Experimental

The automated reactor was set up according the schematic shown in Figure S2. Each reagent was pumped using Jasco PU-980 dual piston pumps and were mixed in Swagelok 316 stainless steel tee-pieces (SS-100-3). A 3 mL reactor coil was fitted to the mantle of a Polar Bear Plus Flow Synthesiser (Cambride Reactor Design). The reaction feed exited the reactor through a Swagelok 316 stainless steel inline filter (SS-2F-15) to a VICI Valco sample loop (EUDA) fitted with a 0.06 µL sampling valve (CI4W.06). The reactor was maintained under a back pressure of 250 psi by an Upchurch Scientific fixed pressure BPR. PTFE tubing (1/16" OD, 1/32" ID, Polyflon) was used throughout. HPLC analysis was carried out using an Agilent 1100. Pump solution reservoirs were prepared by dissolving the reagents in a mixture of acetonitrile and water (7:2, v:v) except the acid chloride **2**, which was prepared in anhydrous acetonitrile. Aniline **4** solution was filtered to remove particulates before use.

3.1   Pump Reservoir Solutions

Pumps A and B: The desired reagents were dissolved in acetonitrile and water (7:2, v:v, MeCN:H_2O) under stirring at ambient conditions. Aniline **4** solution was filtered before use. Pump C: 3-chloropropionyl chloride was added to a dry quick-fit conical flask, fitted with a septum and purged with nitrogen. Anhydrous acetonitrile was added under stirring and nitrogen flow. The solutions were prepared according to the concentrations in Table S1.

Table S1 - Concentrations of the stock solutions for both optimizations

	Pump A		Pump B		Pump C	
	Reagent	Concentration / mol L^{-1}	Reagent	Concentration / mol L^{-1}	Reagent	Concentration / mol L^{-1}
Model	Aniline **4** Biphenyl	0.241 0.0156	Et$_3$N	3.73	Acid chloride **2**	1.00
AZD9291	Aniline **1** HCl Biphenyl	0.136 0.109 0.0255	Et$_3$N	1.20	Acid chloride **2**	0.500

3.2   Model Optimization Results

3.2.1   *N*-(2,4-dimethoxyphenyl)prop-2-enamide, 6
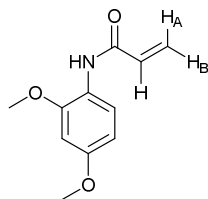
A standard for HPLC analysis was synthesized using the following procedure: 2,4-dimethoxy aniline (498 mg, 3.25 mmol) and triethylamine (1.15 mL, 8.26 mmol) were dissolved in acetonitrile. The black mixture was cooled to 0 °C (aq ice bath) and 3-chloropronionyl chloride (0.47 mL, 4.92 mmol) was added drop-wise with rigorous stirring. The reaction was stirred at 0 °C for 3 hours and then quenched with HCl (2M, 10 mL). Acetonitrile was removed under vacuum and the resultant residue was washed with dichloromethane (3 x 10 mL) The organic fractions were combined and washed with HCl (2M, 3 x 10 mL) and then dried (Na_2SO_4) and concentrated under vacuum to leave the crude product as a black flaky solid. Crystalizing from EtOAc–hexane gave the acrylamide (512 mg, 76%, 94 % purity) as dark brown plates, mp 119-121 °C; δ_H (500 MHz, $CDCl_3$, $SiMe_4$) 8.36 (1H, d, J 9.0, aryl 6-H), 7.68 (1H, br s, N-H), 6.48-6.50 (2H, m, aryl 3-H and 5-H), 6.40 (1H, dd, J 17.0 and 1.0, allyl 3-H_A), 6.27 (1H, dd, J 16.5 and 10.0, allyl 2-H) 5.72 (1H, dd, J 10.0 and 1.0, allyl 3-H_B), 3.87 (3H, s, methoxy 2-CH_3), 3.80 (3H, s, methoxy 4-CH_3); δ_C (125 MHz, $CDCl_3$, $SiMe_4$) 163.0 (aryl 4-C), 156.5 (CO), 149.2 (aryl 2-C), 133.0 (allyl 2-C), 131.6 (allyl 3-C), 121.2 (aryl 1-C), 120.8 (aryl 6-C), 103.8 (aryl 5-C), 98.6 (aryl 3-C) 55.7 (methoxy 2-C), 55.5 (methoxy 4-C); v_{max}/cm^{-1} (solid); 1453, 1467, 1506, 1536, 1612, 1652, 2942, 2973, 3010, 3233; m/z (ESI+) found $[M+H]^+$ 208.0968, $C_{11}H_{14}NO_3$ requires $[M+H]^+$ 208.0968.

3.2.2 Model Acrylamide Optimization

The optimization was carried out according to the limits described in Table S2 using the reactor described in Figure S2. The data from the optimization is displayed in Table S3.

Table S2 - Optimization limits used in the model compound self-optimization

Limits	**4** flow / mL min^{-1}	NEt_3 eq	**2** eq	Temperature / °C
Upper	0.100	4.5	0.9	0
Lower	0.400	20	2.1	130

*Table S3 – List of conditions and response of **6** for the model compound optimization. Optimum conditions are highlighted in green.*

Entry	**4** / mL min^{-1}	**2** / eq	NEt_3 / eq	Temperature / °C	A_x/A_{IS}	Yield **6** %
1	0.495	1.0	7.1	0.1	1.86	26.2

Entry	4 / mL min^{-1}	2 / eq	NEt$_3$ / eq	Temperature / °C	A_x/A_{IS}	Yield 6 %
2	0.369	1.8	15.5	63.4	2.34	35.2
3	0.333	1.9	8.0	96.7	2.43	38.8
4	0.214	1.3	5.3	130.0	2.63	41.9
5	0.480	1.9	13.2	16.0	2.34	35.7
6	0.120	1.2	11.3	31.8	3.26	65.1
7	0.340	1.2	11.3	80.9	2.65	45.3
8	0.360	0.9	6.7	113.4	2.67	47.7
9	0.180	1.5	7.8	47.7	2.94	49.6
10	0.490	1.2	7.3	71.6	2.08	30.0
11	0.490	1.6	12.6	105.4	2.53	39.9
12	0.470	1.1	9.8	121.6	2.90	56.0
13	0.500	0.9	8.6	13.1	1.94	30.4
14	0.100	1.2	4.8	54.2	2.82	46.3
15	0.220	1.7	9.2	64.2	2.93	49.2
16	0.500	1.5	14.8	130.0	3.22	68.7
17	0.100	1.5	15.2	23.4	3.58	77.3
18	0.100	1.5	14.8	80.9	3.53	85.1
19	0.200	1.7	13.9	80.9	3.48	67.9
20	0.360	1.8	17.7	130.0	3.46	77.7
21	0.340	1.5	14.8	130.0	3.55	80.2
22	0.100	2.0	14.6	0.0	3.71	77.0
23	0.100	1.9	18.5	7.5	3.69	79.1
24	0.320	1.2	6.6	76.6	2.20	31.4
25	0.100	2.0	18.0	84.4	3.61	71.3
26	0.100	1.7	13.8	0.0	3.73	75.6
27	0.100	1.9	15.3	76.3	3.79	77.5
28	0.100	2.1	15.5	79.9	3.74	75.4
29	0.150	1.2	9.8	105.5	3.44	64.8
30	0.220	1.2	11.9	130.0	3.77	91.1
31	0.200	1.0	8.7	15.9	3.00	51.5
32	0.100	2.1	19.5	74.8	3.53	81.1
33	0.100	1.4	9.9	82.7	3.56	69.1
34	0.100	1.8	12.9	89.2	3.64	71.7
35	0.100	1.7	16.3	117.8	3.82	91.9
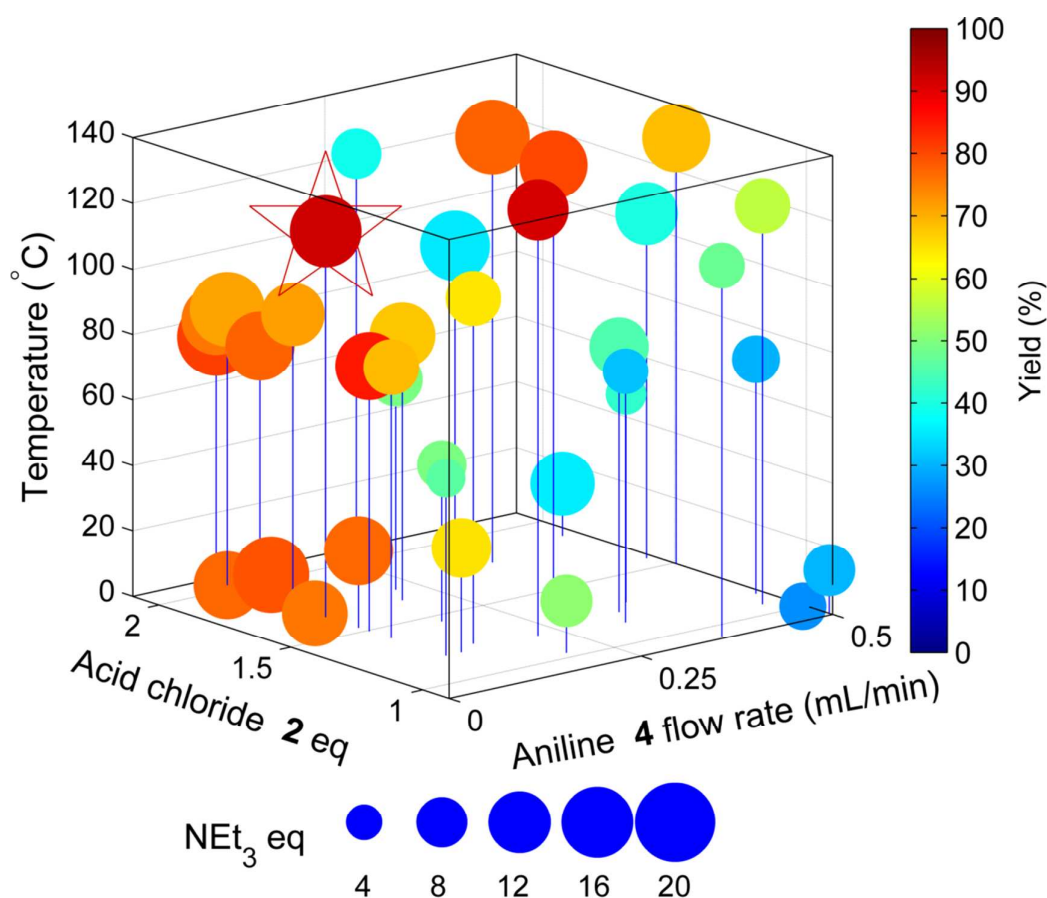
*Figure S6 - Multi-dimensional plot of the optimization of acrylamide **6**. The 3-axis plot show the aniline **4** flow rate (x-axis), acid chloride **2** eq (y-axis) and temperature (z-axis). The size of the point represents the eq of NEt₃, and the color represents the product yield. The optimum conditions: 12.2 min, 117.8 °C, 16 eq NEt₃, 1.7 eq **2** are highlighted by the star*

3.2.3 Impurity Results

The composition of the major impurities (maximum HPLC area ≥ 1%) is shown in Table for the conditions shown in Table S3. A visual representation showing the area of experimental space where the yield is highest is shown in Figure S7.

Table S4 – Composition of products for each experiment shown in Table S3.

Entry	Conditions				Yield / %			
	4 / mL min^{-1}	**2** / eq	NEt₃ / eq	Temperature / °C	**4**	**5**	**7**	**8**
1	0.495	1.0	7.1	0.1	0.0	68.4	4.4	0.5
2	0.369	1.8	15.5	63.4	0.0	58.2	5.5	0.4
3	0.333	1.9	8.0	96.7	0.3	54.0	5.7	0.4
4	0.214	1.3	5.3	130.0	0.0	51.0	6.3	0.6

Entry	Conditions				Yield / %			
	4 / mL min^{-1}	**2** / eq	NEt$_3$ / eq	Temperature / °C	**4**	**5**	**7**	**8**
5	0.480	1.9	13.2	16.0	0.0	57.6	5.5	0.6
6	0.120	1.2	11.3	31.8	0.5	21.1	12.6	0.8
7	0.340	1.2	11.3	80.9	0.3	47.6	6.1	0.5
8	0.360	0.9	6.7	113.4	0.5	47.1	3.8	0.6
9	0.180	1.5	7.8	47.7	0.0	39.3	9.3	0.6
10	0.490	1.2	7.3	71.6	0.0	63.7	5.0	0.3
11	0.490	1.6	12.6	105.4	0.0	54.4	4.7	0.4
12	0.470	1.1	9.8	121.6	0.7	40.4	1.6	0.5
13	0.500	0.9	8.6	13.1	0.5	63.0	5.3	0.4
14	0.100	1.2	4.8	54.2	0.0	42.7	9.6	0.5
15	0.220	1.7	9.2	64.2	0.0	40.8	8.7	0.5
16	0.500	1.5	14.8	130.0	0.4	28.2	1.4	0.7
17	0.100	1.5	15.2	23.4	0.5	6.4	15.0	0.9
18	0.100	1.5	14.8	80.9	0.5	3.5	9.9	0.9
19	0.200	1.7	13.9	80.9	0.0	21.4	10.0	0.7
20	0.360	1.8	17.7	130.0	0.3	19.1	1.5	0.8
21	0.340	1.5	14.8	130.0	0.5	17.1	0.9	0.8
22	0.100	2.0	14.6	0.0	0.0	7.8	13.9	0.6
23	0.100	1.9	18.5	7.5	0.0	5.7	14.4	0.8
24	0.320	1.2	6.6	76.6	0.0	62.0	5.5	0.3
25	0.100	2.0	18.0	84.4	0.0	15.8	12.2	0.7
26	0.100	1.7	13.8	0.0	0.0	8.6	14.6	0.9
27	0.100	1.9	15.3	76.3	0.0	7.1	14.1	0.8
28	0.100	2.1	15.5	79.9	0.0	10.2	13.1	0.8
29	0.150	1.2	9.8	105.5	0.0	23.5	10.3	0.7
30	0.220	1.2	11.9	130.0	1.0	5.4	0.8	1.0
31	0.200	1.0	8.7	15.9	0.0	36.9	9.9	0.6
32	0.100	2.1	19.5	74.8	0.0	4.9	12.6	0.8
33	0.100	1.4	9.9	82.7	0.0	16.7	13.0	0.7
34	0.100	1.8	12.9	89.2	0.0	13.9	13.2	0.7
35	0.100	1.7	16.3	117.8	0.0	2.7	3.9	0.9
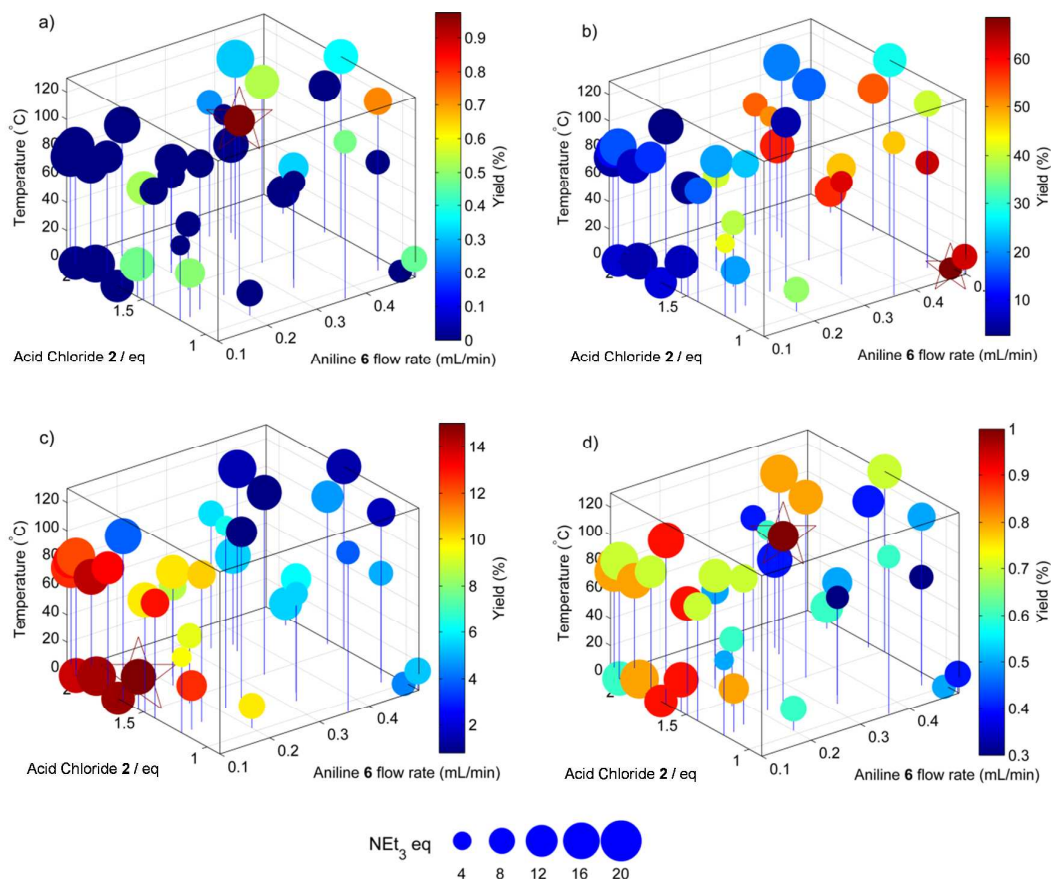
*Figure S7 – Impurity maps showing the compositions of the major impurities: aniline **4** (a), chloroamide **5** (b), enolate **7** (c) and dimer **8** (d).*

3.2.4 Impurity Identification with LCMS
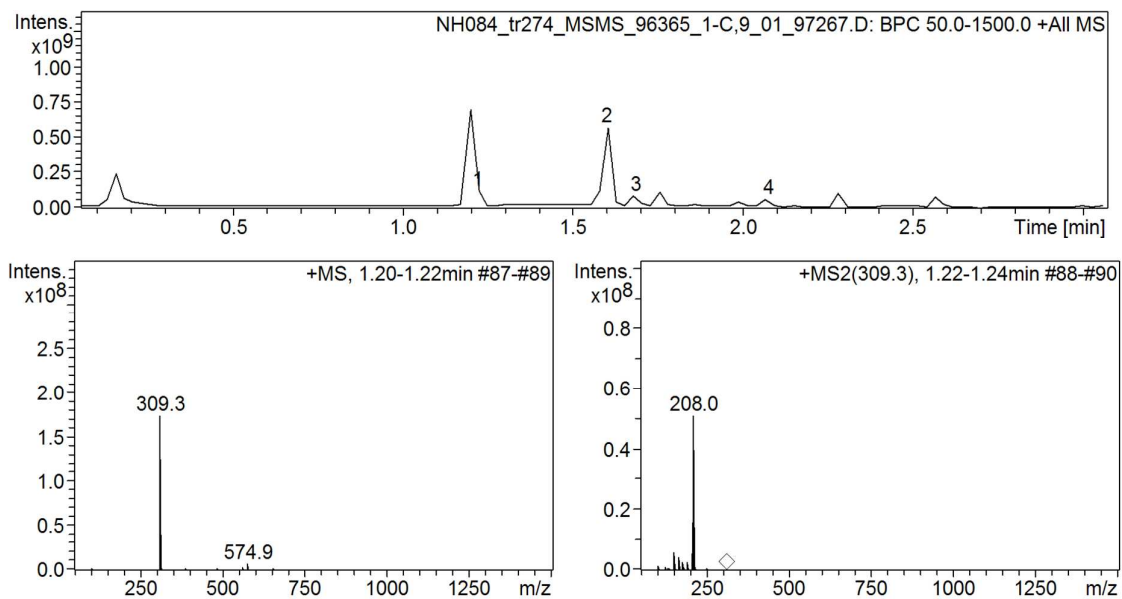
*Figure S8 – LC XIC chromatogram (above) and MS-MS spectra of compound t_R 1.22 min (below). Analysis determined that the peak was enolate **7** (other compounds: 1 is acrylamide **6**, 3 is chloroamide **5**)*
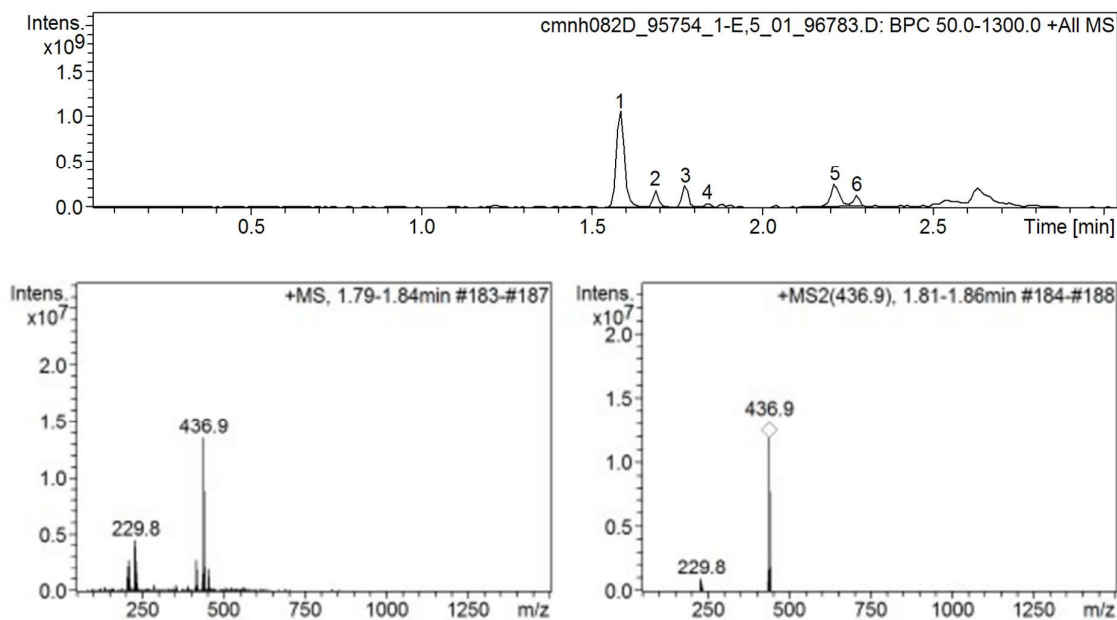
*Figure S9 – LC XIC chromatogram (above) and MS-MS spectrum of compound t_R 1.80 min (below). Structural analysis determined that the peak corresponded to dimer **8** (1 is acrylamide **6**, 3 is chloroamide **5**).*

3.2.5 Enolate Optimization

Another optimization was run, to maximize the amount of **7**, and find experimental regions where the impurity formation is high. The yields of by-product **7** from the original optimization (Table S3 and Figure S6) were inputted to SNOBFIT as preliminary data and the algorithm continued from the last data set. The results from the additional optimization are shown below in Table S5.

It should be expected that the optimum region of **7** (Figure S10) is similar to that of the acrylamide **6**, as the acrylamide is a precursor for the formation of the enolate. However, **7** is formed in higher yields at much lower temperatures, suggesting two possibilities for it formation. Firstly, as the reaction from **6** to **7** (Scheme 2) is likely to be reversible, it is possible that increased temperatures favor the acrylamide **6** in the equilibrium. Secondly, it could be that increased temperatures favor the onward reaction of **7** with another molecule of **6**, resulting in the formation of the dimer **8b** – although LC-MS analysis strongly suggests this route is not favored.
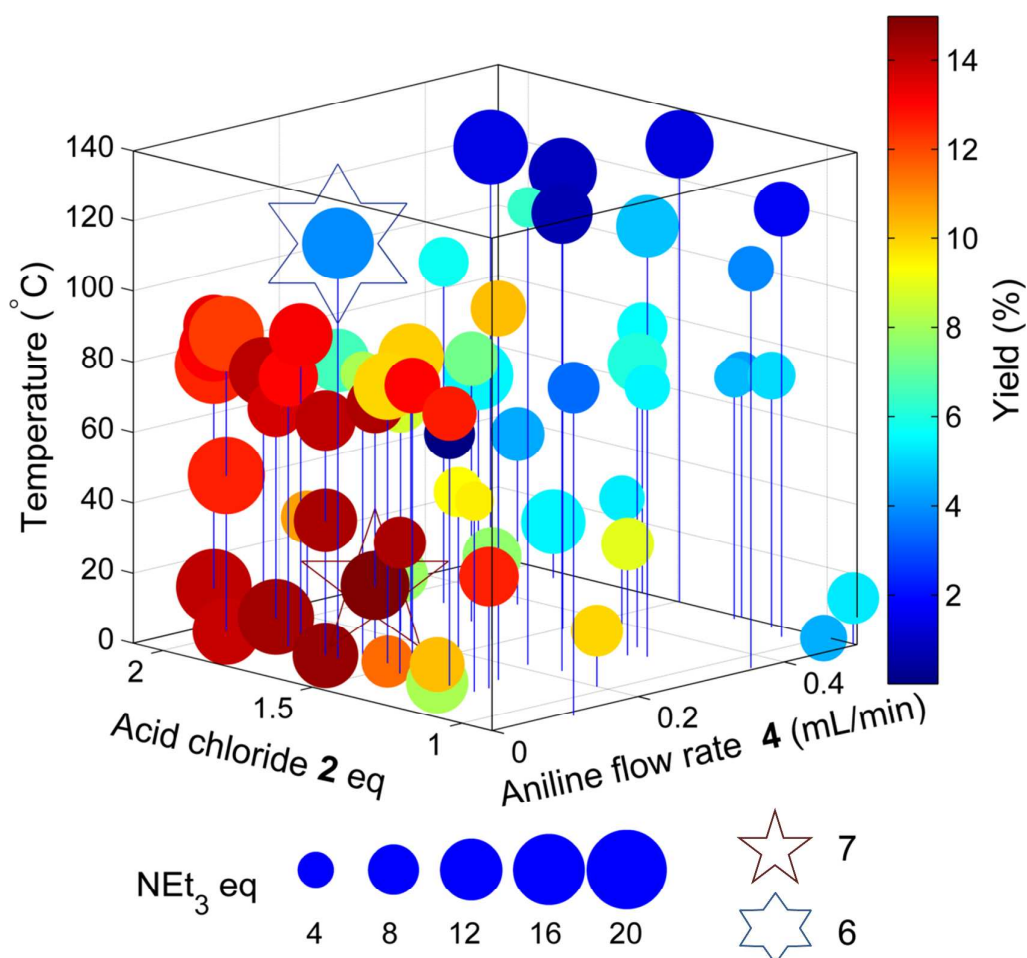
*Figure S10 - Multi-dimensional plot, showing the results of the optimization of enolate **7**. The 3-axis plot show the aniline **4** flow rate (x-axis), acid chloride **2** eq (y-axis) and temperature (z-axis). The size of the point represents NEt$_3$ eq, and the colour represents the product yield. The optimum conditions: 0.1 mL min^{-1} **4**, 117.8 °C, 1.5 eq **2**, 15.2 eq NEt$_3$ and 12.7 min are highlighted by the 5-pointed star. The optimum conditions of **6** are highlighted by the 6-pointed star.*

*Table S5 – List of conditions and response for the optimization of enolate **7**. The original conditions and response from the first optimization are greyed out. The optimum conditions are highlighted in green*

Entry	**4** / mL min^{-1}	**2** / eq	NEt$_3$ / eq	Temperature / °C	A$_x$/A$_{IS}$	Yield **7** %
1	0.495	1.0	7.1	0.1	0.31	4.4
2	0.214	1.3	5.3	130.0	0.40	6.2
3	0.369	1.8	15.5	63.4	0.37	5.5

Entry	4 / mL min^{-1}	2 / eq	NEt$_3$ / eq	Temperature / °C	A$_x$/A$_{IS}$	Yield 7 %
4	0.333	1.9	8.0	96.7	0.36	5.7
5	0.480	1.9	13.2	16.0	0.36	5.4
6	0.120	1.2	11.3	31.8	0.63	12.5
7	0.340	1.2	11.3	80.9	0.36	6.0
8	0.360	0.9	6.7	113.4	0.21	3.7
9	0.180	1.5	7.8	47.7	0.55	9.3
10	0.490	1.2	7.3	71.6	0.35	5.0
11	0.490	1.6	12.6	105.4	0.30	4.7
12	0.470	1.1	9.8	121.6	0.09	1.6
13	0.500	0.9	8.6	13.1	0.34	5.3
14	0.100	1.2	4.8	54.2	0.58	9.5
15	0.220	1.7	9.2	64.2	0.52	8.6
16	0.500	1.5	14.8	130.0	0.07	1.4
17	0.100	1.5	15.2	23.4	0.69	14.7
18	0.100	1.5	14.8	80.9	0.41	9.7
19	0.200	1.7	13.9	80.9	0.52	9.8
20	0.360	1.8	17.7	130.0	0.06	1.4
21	0.340	1.5	14.8	130.0	0.04	0.9
22	0.100	2.0	14.6	0.0	0.67	13.7
23	0.100	1.9	18.5	7.5	0.67	14.1
24	0.320	1.2	6.6	76.6	0.38	5.4
25	0.100	2.0	18.0	84.4	0.62	11.9
26	0.100	1.7	13.8	0.0	0.72	14.4
27	0.100	1.9	15.3	76.3	0.69	13.7
28	0.100	2.1	15.5	79.9	0.65	12.8
29	0.150	1.2	9.8	105.5	0.54	10.1
30	0.220	1.2	11.9	130.0	0.03	0.7
31	0.200	1.0	8.7	15.9	0.58	9.9
32	0.100	2.1	19.5	74.8	0.55	12.2
33	0.100	1.4	9.9	82.7	0.67	12.8
34	0.100	1.8	12.9	89.2	0.67	12.9
35	0.100	1.7	16.3	117.8	0.16	3.8
36	0.100	1.3	12.4	0.0	**0.26**	8.1
37	0.260	1.5	11.1	23.8	0.50	7.7
38	0.100	1.7	12.8	38.4	0.73	14.1

Entry	4 / mL min^{-1}	2 / eq	NEt$_3$ / eq	Temperature / °C	A$_x$/A$_{IS}$	Yield 7 %
39	0.100	1.5	10.5	74.7	0.73	14.1
40	0.100	0.9	8.6	93.3	0.12	3.4
41	0.100	1.5	8.6	2.5	0.62	11.4
42	0.100	1.3	9.6	5.1	0.56	10.2
43	0.160	1.9	8.9	32.1	0.57	10.7
44	0.100	1.9	10.4	66.7	0.68	13.5
45	0.370	1.4	6.6	38.3	0.37	5.3
46	0.100	2.0	18.9	44.3	0.64	12.3
47	0.100	1.7	11.7	66.7	0.68	13.7
48	0.100	2.1	11.9	85.9	0.65	13.0
49	0.100	2.1	18.2	11.8	0.67	13.6
50	0.100	1.5	8.7	37.3	0.72	14.1
51	0.380	1.7	9.2	48.3	0.29	4.3
52	0.100	1.3	8.3	71.5	0.00	0.0
53	0.100	1.6	6.3	82.7	0.49	8.1
54	0.310	1.2	8.9	31.8	0.53	8.9
55	0.490	1.3	5.2	68.5	0.33	4.6
56	0.300	1.7	9.5	74.5	0.44	7.2
57	0.500	1.6	8.1	75.2	0.38	5.5
58	0.100	1.8	11.2	76.5	0.68	12.7
59	0.220	1.7	9.6	16.1	0.48	7.8
60	0.270	2.1	12.9	67.7	0.39	6.4
61	0.500	1.3	5.6	69.5	0.30	4.2
62	0.100	1.3	9.4	77.3	0.66	12.5

3.3 AZD9291 Optimization

The Optimization of **3** was carried out according to the limits displayed in Table S6. A list of conditions and responses from the optimization are displayed in

Table S6 – Boundary limits for the optimization of 3

Limit	4 flow / mL min^{-1}	NEt$_3$ eq	2 eq	Temperature / °C
Minimum	0.080	2.2	0.75	80
Maximum	0.150	15	3.0	150

*Table S7 – List of conditions and responses for the optimization of **3**. Optimum conditions are highlighted in green.*

Entry	1 / mL min^{-1}	2 / eq	NEt$_3$ / eq	Temperature / °C	A$_x$/A$_{IS}$	Yield 3 %
1	0.100	1.3	5.0	80.1	1.80	37.1
2	0.118	2.4	9.4	149.8	2.87	68.0
3	0.130	0.9	3.7	141.1	2.97	53.7
4	0.100	1.9	5.0	105.4	3.52	72.3
5	0.120	1.0	3.3	106.3	2.37	47.3
6	0.080	0.8	2.2	150.0	1.99	55.8
7	0.150	1.9	8.6	150.0	2.93	67.8
8	0.080	0.8	2.6	93.6	1.80	41.1
9	0.080	2.8	7.6	99.6	3.82	79.4
10	0.080	2.4	6.3	107.1	2.69	57.1
11	0.100	1.4	5.4	119.4	1.98	51.1
12	0.150	0.8	2.6	147.6	2.21	51.3
13	0.090	3.0	9.5	88.2	2.70	71.2
14	0.120	2.4	6.5	104.4	3.23	77.1
15	0.110	3.0	8.0	106.1	3.59	82.3
16	0.110	2.7	10.5	123.9	4.49	88.9
17	0.120	1.0	3.3	86.6	2.15	48.8
18	0.100	0.9	2.5	106.3	2.41	56.7
19	0.110	1.8	4.8	124.0	3.18	83.2
20	0.090	3.0	9.9	124.2	3.86	85.6
21	0.080	1.8	4.7	103.0	3.34	75.1
22	0.100	1.4	6.7	110.9	2.81	69.3
23	0.130	3.0	13.8	123.3	4.29	83.2
24	0.090	2.4	6.4	123.3	3.47	81.6
25	0.120	3.0	14.9	141.1	3.77	75.7
26	0.100	3.0	10.6	111.0	3.14	74.0
27	0.090	3.0	13.6	124.1	3.35	74.7
28	0.140	3.0	11.4	138.3	3.77	81.0
29	0.110	1.3	4.3	145.6	3.36	72.0
30	0.120	1.1	5.3	121.7	2.49	61.6
31	0.150	3.0	10.9	123.4	3.69	80.7
32	0.130	3.0	11.1	124.1	3.84	86.5

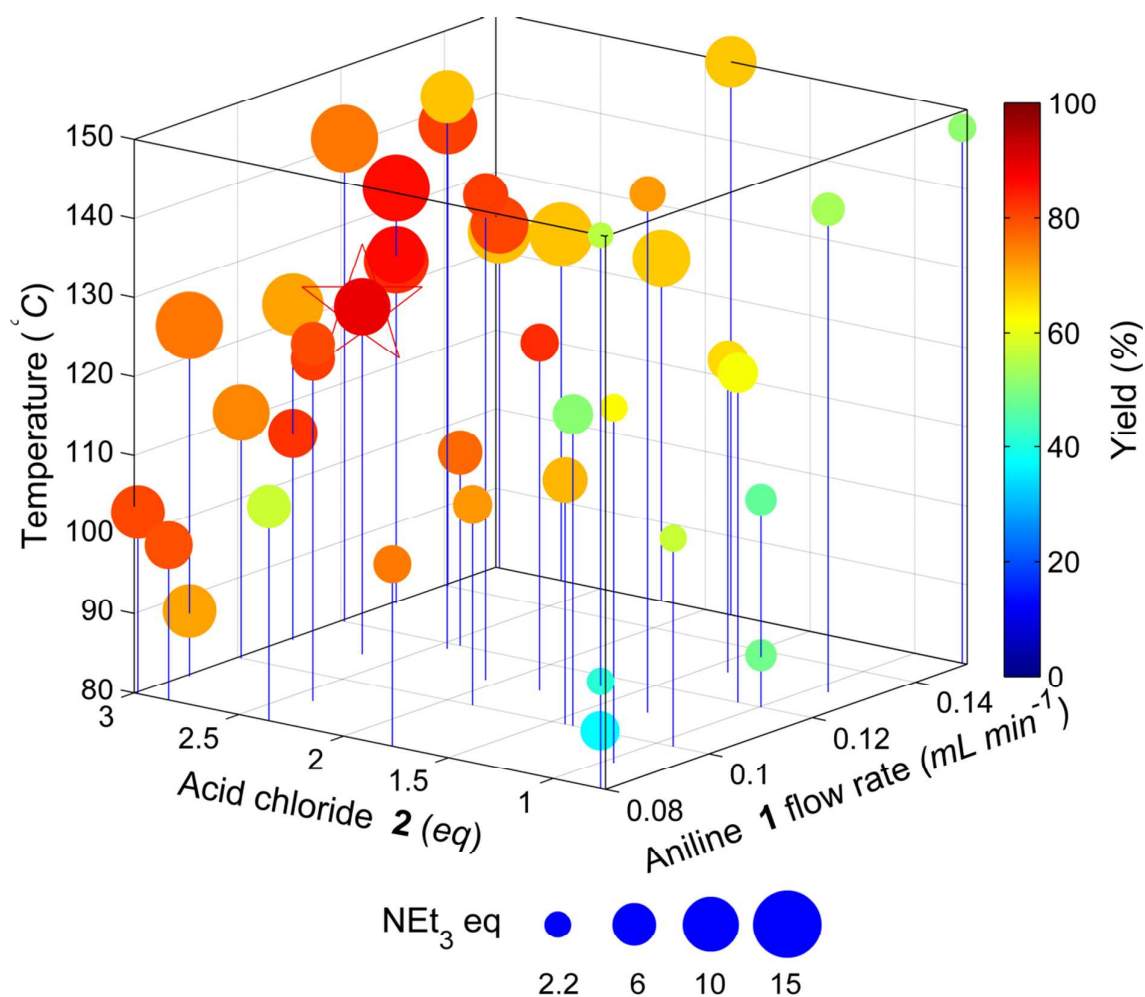| Entry	1 / mL min^{-1}	2 / eq	NEt$_3$ / eq	Temperature / °C	A_x/A_{IS}	Yield 3 %
33	0.130	3.0	14.9	132.6	3.39	86.1
34	0.080	3.0	9.5	103.0	3.93	80.1
35	0.150	3.0	13.1	122.5	3.34	68.5
36	0.090	1.0	2.6	124.9	2.82	62.8
37	0.090	2.4	6.4	125.2	3.37	79.9
38	0.110	2.1	6.7	141.2	3.25	81.3
39	0.130	1.4	5.4	119.4	2.58	65.7
40	0.110	3.0	12.4	122.4	3.56	71.5
41	0.150	2.2	11.0	123.3	2.83	67.3
42	0.150	2.7	13.4	123.8	2.47	68.0

*Figure S11 - Multidimensional plot of the optimization of acrylamide **3**. The 3 axis flow rate shows the aniline **1** flow rate (x-axis), acid chloride **2** eq (y-axis) and temperature (z-axis).*

The size of the point corresponds to the triethylamine eq, the color is the yield. Optimum conditions: 9.36 min, 123.9 °C, 10.5 eq NEt₃, 2.7 eq 2 are highlighted by the star.

3.3.1 AZD9291 Impurity Results

Entry	Conditions				Yield / %					
	1 / mL min⁻¹	**3** / eq	NEt₃ / eq	Temp / °C	Imp 1	**1**	Dimer	Chloro-amide	Imp 2	Imp 3
1	0.100	1.3	5.0	80.1	0.3	57.3	1.6	1.2	0.0	0.4
2	0.118	2.4	9.4	149.8	0.3	21.4	4.7	3.1	0.0	0.4
3	0.130	0.9	3.7	141.1	1.9	39.9	0.3	0.0	0.0	0.6
4	0.100	1.9	5.0	105.4	0.3	14.1	4.2	1.8	0.0	0.8
5	0.120	1.0	3.3	106.3	0.6	44.6	2.1	0.6	0.3	0.6
6	0.080	0.8	2.2	150.0	3.0	34.3	0.9	0.0	0.0	0.8
7	0.150	1.9	8.6	150.0	0.7	25.9	0.4	0.0	0.3	0.6
8	0.080	0.8	2.6	93.6	0.7	48.5	2.3	0.6	0.3	0.8
9	0.080	2.8	7.6	99.6	0.0	5.1	6.7	4.0	0.6	0.7
10	0.080	2.4	6.3	107.1	0.4	29.8	2.1	2.1	1.3	0.6
11	0.100	1.4	5.4	119.4	0.8	41.4	0.7	0.4	0.6	1.3
12	0.150	0.8	2.6	147.6	1.4	40.8	0.4	0.4	0.2	0.8
13	0.090	3.0	9.5	88.2	0.3	12.3	4.2	4.5	0.7	0.7
14	0.120	2.4	6.5	104.4	0.4	5.7	4.4	3.6	0.6	0.6
15	0.110	3.0	8.0	106.1	0.3	1.3	4.6	4.6	0.5	0.7
16	0.110	2.7	10.5	123.9	0.0	2.6	1.8	1.1	1.2	0.8
17	0.120	1.0	3.3	86.6	0.2	39.2	2.4	1.4	0.6	0.8
18	0.100	0.9	2.5	106.3	0.8	33.3	2.5	0.7	0.3	1.0
19	0.110	1.8	4.8	124.0	0.4	7.8	1.1	0.7	0.4	0.7
20	0.090	3.0	9.9	124.2	0.5	4.6	0.9	1.3	0.7	0.8
21	0.080	1.8	4.7	103.0	0.3	9.3	4.7	2.0	0.8	0.8
22	0.100	1.4	6.7	110.9	0.4	18.3	2.7	1.4	0.7	0.9
23	0.130	3.0	13.8	123.3	0.0	6.9	2.2	1.7	1.1	0.9
24	0.090	2.4	6.4	123.3	0.4	8.9	0.9	0.8	0.6	0.8
25	0.120	3.0	14.9	141.1	0.0	15.4	1.0	0.8	0.8	0.8
26	0.100	3.0	10.6	111.0	0.0	11.2	3.0	3.1	1.0	0.7
27	0.090	3.0	13.6	124.1	0.0	14.9	0.7	2.1	1.1	0.8
28	0.140	3.0	11.4	138.3	0.0	10.4	0.5	1.0	0.8	1.2
29	0.110	1.3	4.3	145.6	1.2	19.3	0.4	0.3	0.0	1.0

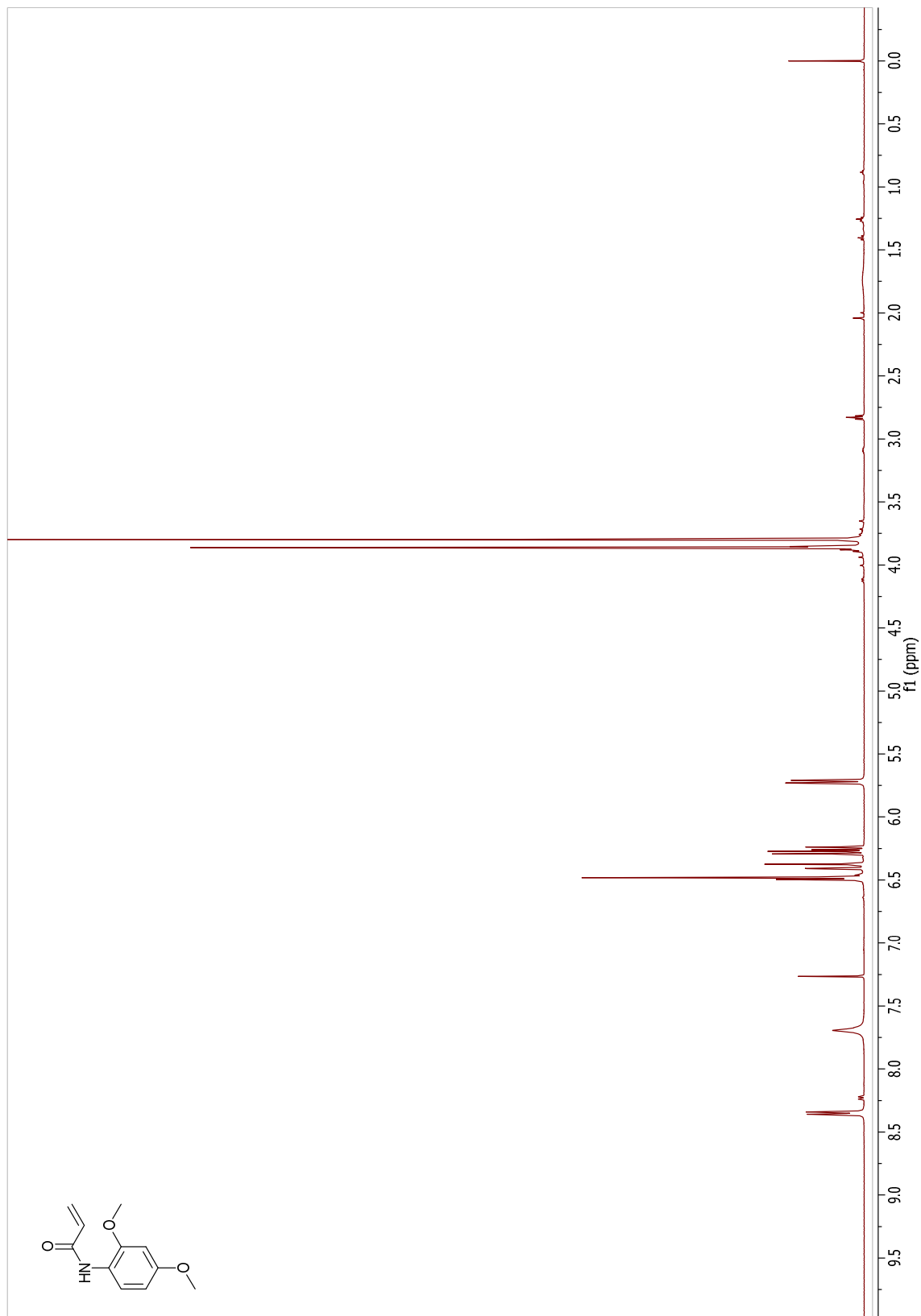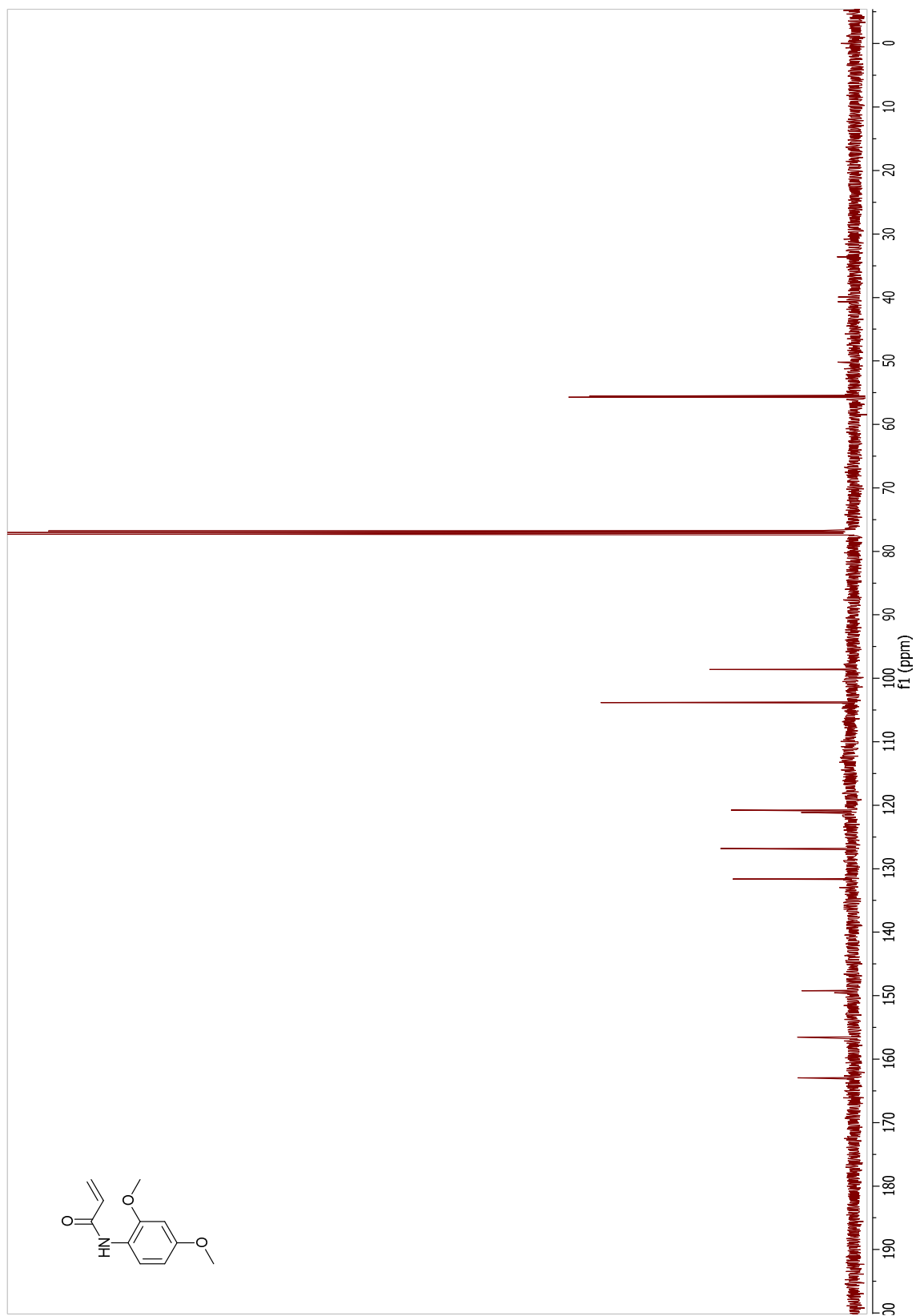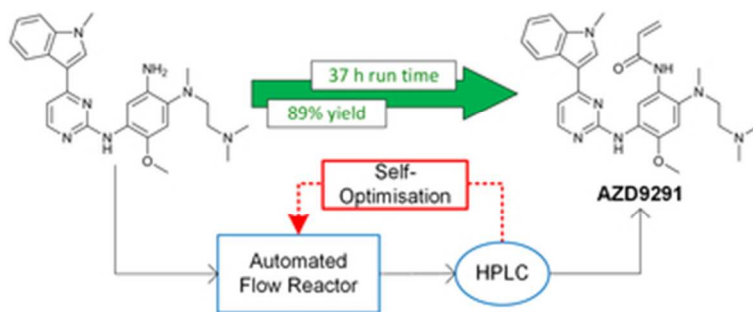| Entry	Conditions				Yield / %					
	1 / mL min^{-1}	**3** / eq	NEt$_3$ / eq	Temp / °C	Imp 1	**1**	Dimer	Chloro-amide	Imp 2	Imp 3
30	0.120	1.1	5.3	121.7	0.7	29.5	0.7	0.5	0.6	1.0
31	0.150	3.0	10.9	123.4	0.0	7.2	1.7	2.3	1.3	0.8
32	0.130	3.0	11.1	124.1	0.0	3.5	1.5	1.8	1.0	0.9
33	0.130	3.0	14.9	132.6	0.0	4.1	0.7	1.4	1.2	0.7
34	0.080	3.0	9.5	103.0	0.0	3.9	4.8	3.3	0.8	1.1
35	0.150	3.0	13.1	122.5	0.0	18.6	1.5	2.1	1.0	0.9
36	0.090	1.0	2.6	124.9	1.4	27.0	0.6	0.2	0.8	1.1
37	0.090	2.4	6.4	125.2	0.5	9.4	0.8	0.8	0.9	0.9
38	0.110	2.1	6.7	141.2	0.5	10.7	0.7	0.0	0.4	1.4
39	0.130	1.4	5.4	119.4	0.4	22.9	1.1	1.0	0.7	0.9
40	0.110	3.0	12.4	122.4	0.0	16.2	1.0	1.5	1.1	1.4
41	0.150	2.2	11.0	123.3	0.0	21.3	1.1	1.6	1.0	1.0
42	0.150	2.7	13.4	123.8	0.0	20.2	1.0	1.2	0.9	1.0
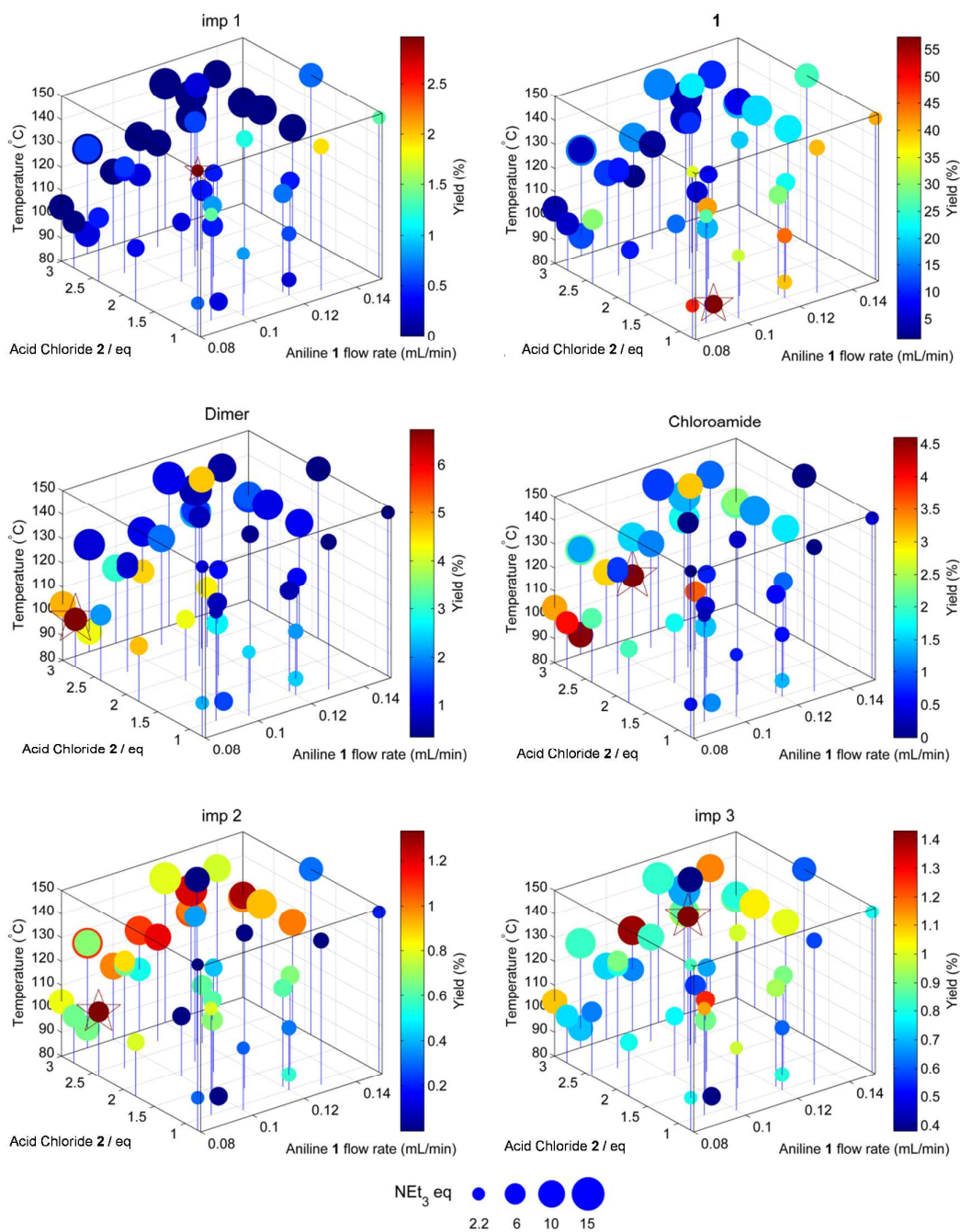
Figure S12 – Impurity maps showing the composition of different products as displayed in Figure S5

S22

32x12mm (300 x 300 DPI)